Available online at www.sciencedirect.com

ScienceDirect

Current Opinion in Electrochemistry

Review Article

First principles calculations of oxygen reduction reaction at fuel cell cathodes

Eugene A. Kotomin[1,2], Yuri A. Mastrikov[1,2], Rotraut Merkle[1] and Joachim Maier[1]

Abstract

The efficiency of solid oxide fuel cells (SOFC) depends critically on materials, in particular for the cathode where the oxygen reduction reaction (ORR) occurs. Typically, mixed conducting perovskite ABO_3-type materials are used for this purpose. The dominating surface terminations are (001) AO and BO_2, with the relative fractions depending on materials composition and ambient conditions.

Here, results of recent large-scale first principles (*ab initio*) calculations for the two alternative polar (La,Sr)O and MnO_2 (001) terminations of (La,Sr)MnO_3 cathode materials are discussed. The surface oxygen vacancy concentration for the (La,Sr)O termination is more than 5 orders of magnitude smaller compared to MnO_2, which leads to drastically decreased estimated ORR rates. Thus, it is predicted for prototypical SOFC cathode materials that the BO_2 termination largely determines the ORR kinetics, although with Sr surface segregation (long-term degradation) its fraction of the total surface area decreases, which slows down cathode kinetics.

Addresses

[1] Max Planck Institute for Solid State Research, Stuttgart, Germany
[2] Institute of Solid State Physics, University of Latvia, Riga, Latvia

Corresponding author: Kotomin, Eugene A (E.Kotomin@fkf.mpg.de)

Current Opinion in Electrochemistry 2020, **19**:122–128

This review comes from a themed issue on **Fundamental and Theoretical Electrochemistry**

Edited by **Galina Tsirlina**

For a complete overview see the Issue and the Editorial

Available online 29 November 2019

https://doi.org/10.1016/j.coelec.2019.11.005

Keywords

First principles calculations, Fuel cells, Cathode materials, Polar surfaces, Perovskites, Oxygen reduction Reaction (ORR), Rate determining step.

Introduction

Solid oxide fuel cells (SOFC) allow for clean efficient conversion of chemical to electrical energy, in particular also in comparably small devices (several kW), see for example, Ref. [1]. The kinetics of the oxygen reduction reaction (ORR) becomes increasingly important with decreasing operation temperature. The ORR kinetics has been intensively investigated by experiments and *ab initio* calculations (see e.g., reviews [2–7]): (i) $La_{1-x}Sr_xMnO_{3-\delta}$ (LSM) as one of the first ABO_3-type hole and oxygen vacancy ($V_O^{\bullet\bullet}$) mixed conducting perovskites employed as SOFC cathode, and (ii) $La_{1-x}Sr_xCo_{1-y}Fe_yO_{3-\delta}$ (LSCF) with significantly higher $V_O^{\bullet\bullet}$ concentration as second-generation materials.

The ORR is a multistep reaction that comprises molecular chemisorption (formation of adsorbed superoxide O_2^-, peroxide O_2^{2-}), O–O bond dissociation, and incorporation of oxygen species into surface $V_O^{\bullet\bullet}$ of the cathode material. Typically, one of these steps is much slower than the others and plays the role of the rate-determining step (rds), which defines the overall ORR rate. While certain information on the ORR mechanism and the rds can be extracted from experimental data (e.g., dependence of ORR rate on pO_2 and dopant/defect concentrations [8]), *ab initio* (first principles) calculations are an important complementary tool. They allow one to determine defect formation energies and migration barriers, which differ from bulk values, and supply transition state energies. Usually, idealized model surfaces are assumed. For ABO_3 perovskites, low-index (001) AO and BO_2 surfaces typically represent the lowest energy terminations. Their relative fractions depend on material composition [9], T, pO_2, and thermal history (higher Sr content and/or an increased ratio of A-site to B-site cations), and is closely related to their electrochemical performance (see e.g., Refs. [9–13]). For $La_{1-x}Sr_xMnO_{3-\delta}$ and $La_{1-x}Sr_xCo_{1-y}Fe_yO_{3-\delta}$, the situation is further complicated due to the fact that in general these terminations represent polar surfaces. The physics and chemistry of oxide polar surfaces are summarized in reviews [14,15]. Polar surfaces are electrostatically unstable ("polar catastrophe" due to infinite dipole moment) and must compensate the surface charge by surface rumpling, reconstruction, or charged defect accumulation (e.g., Refs. [16,17]).

The ORR kinetics has been computationally studied first for the BO_2 termination (see e.g., Refs. [18,19] and references therein). Only recently also the AO termination—which for LSM becomes increasingly more

stable with higher Sr content [9]—was also investigated in detail (e.g., Refs. [20–22]). In this paper, we discuss the ORR kinetics of LSM [18,21] and LSC [22] estimated from *ab initio* calculated defect concentrations and migration/reaction barriers, with special emphasis on the effect of the different *A*O and BO_2 terminations and the average oxidation state of the *B*-site cation.

Computational approaches

The computational density functional theory (DFT) methodology [23] for perovskites containing open shell transition metal cations has evolved over recent years from GGA exchange-correlation functionals [24] (e.g., in Ref. [18], and still used in Ref. [21] for comparability with preceding data) to GGA + U (e.g. Refs. [22,25–27]) and present state-of-the-art hybrid functional approaches (e.g., [28] and references therein). While these different functionals yield different absolute energies, the relative sequence of defect formation energies and reaction barriers is expected to be correct.

Sufficiently large supercells must be charged to avoid unintentional interactions of closely spaced defects such as $V_O^{\bullet\bullet}$, and address realistic defect concentrations. If bulk and slabs or perfect and defective materials prefer different types of lattice distortion, care must be taken to avoid or separate such phase transformation energies from the reaction barriers. Similarly, while different types of magnetic order cannot be neglected and lead to different absolute energies, the actual choice of magnetic order is less relevant as long as it remains the same for all studied configurations. To avoid potential artifacts from compensating background charges, it is preferable to always work with neutral supercells, that is, when an O is removed to create a $V_O^{\bullet\bullet}$, two electrons remain behind and are typically accommodated at the transition metal ions.

The surface properties (defects in surface layer, adsorbed molecular and atomic oxygen species, surface reaction energies) are also calculated using a supercell model—a two-dimensional slab infinite in the x,y directions and containing a finite number of planes along the z axis perpendicular to the surface. Typically, 7–8 layer slabs suffice for reasonable convergence of the results (see e.g., Refs. [26,29]). In order to avoid spurious mutual defect or adsorbate interactions, the lateral dimensions must be chosen sufficiently large; the supercell should comprise at least eight times the unit cell area, which corresponds to a surface defect or adsorbate concentration of 0.125 per unit cell.

Symmetrical slabs automatically cancel any overall dipole moment (but local dipoles between surface and second layer may remain), but modify the overall cation A/B ratio and thus possibly the transition metal oxidation state [21], cf. discussion below. On the other hand, asymmetrical slabs as applied for example, in Ref. [22] preserve the A/B ratio but may require additional dipole corrections.

The adsorbate concentrations (coverage) are determined by the adsorption energy and entropy. The latter is negative (loss of degrees of freedom) and can to first approximation be estimated from the experimental gas-phase entropy of O_2 molecule, yielding a contribution of $-T\Delta S^0 \approx 2$ eV at 1000 K [4,18]. Since adsorbed oxygen species are negatively charged, even for highly negative adsorption energies, the mutual Coulombic repulsion limits the coverages to a plateau value in the range of 20% [18,21,30].

From the zero Kelvin DFT calculations, the overall oxidation energy ΔE_{ox} and energies of intermediates and transition states are obtained. To address operational high-temperature conditions, the Gibbs free energies are then calculated taking into account the entropy effects. The largest entropy effect appears for the oxygen adsorption (see earlier discussion). Changes caused by modified vibrational contributions from surface atoms and defects can be also considerable, especially for charged oxygen vacancies [31]. DFT calculations can also be used to explore the thermodynamic stability of cathode materials against decomposition/phase transformations, see for example, Ref. [32]. More computational details can be found in the respective references.

(La,Sr)MnO_3: effect of surface termination on defect and adsorbate concentrations

The effect of *A*O and BO_2 termination was investigated in Ref. [21] on the example of $LaMnO_3$ (LM), $La_{0.75}Sr_{0.25}MnO_3$ (LS25M), and $La_{0.5}Sr_{0.5}MnO_3$ (LS50M). Table 1 summarizes the slab cation compositions and the resulting average Mn oxidation states.

Experimentally, LSM exhibits extremely low bulk $V_O^{\bullet\bullet}$ concentrations below 10^{-7} at SOFC operation conditions, and even formal oxygen excess (= cation vacancies) for low Sr doping [33]. Already for bulk, the Mn oxidation state has a strong effect on the energy of $V_O^{\bullet\bullet}$ formation (= removal of a neutral O accommodating the left-behind two electrons at neighboring Mn). As long as the average Mn oxidation state is $\leq +3.25$, the vacancy formation energy $E_{V_O^{\cdot\cdot}}$ is $\approx$ 4.5 eV, but for larger Mn oxidation states up to +3.6, it strongly decreases approximately linearly to 2.5 eV. Owing to the local structure distortion, $E_{V_O^{\cdot\cdot}}$ for surface vacancies is expected to differ from the bulk values. From the decreased coordination number on the surface layer, one might expect also decreased $E_{V_O^{\cdot\cdot}}$ values. However, the *A*O terminations carry a nominal positive excess charge of $+1e$ (LaO; LM) to $+0.5e$ ($La_{0.5}Sr_{0.5}O$; LS50M), which disfavors $V_O^{\bullet\bullet}$ formation. This increases $E_{V_O^{\cdot\cdot}}$ for the *A*O termination by up to 0.6 eV over the respective

Table 1

Overview data on bulk LSM 2 × 2 × 2 supercells and symmetrical 7-layer (001) slabs, the La/Sr ratio is the same in surface and deeper layers. Data from Ref. [21].

x_{Sr}	Bulk Mn ox. state	Bulk ionic charges/*e*				(La,Sr)O terminated slab		MnO_2 terminated slab	
		La	Sr	Mn	O	Ox. state	Composition	Ox. state	Composition
0	+3.00	2.08		1.71	−1.27	+2.67	$La_4Mn_3O_{10}$	+3.25	$La_3Mn_4O_{11}$
0.25	+3.25	2.09	1.59	1.78	−1.25	+3.00	$La_3SrMn_3O_{10}$	+3.44	$La_{2\cdot25}Sr_{0\cdot75}Mn_4O_{11}$
0.50	+3.50	2.10	1.58	1.83	−1.22	+3.33	$La_2Sr_2Mn_3O_{10}$	+3.63	$La_{1\cdot5}Sr_{1\cdot5}Mn_4O_{11}$

bulk value. On the other hand, the nominal negative excess charge of the MnO_2 termination of −0.75(LM) to −0.37 (LS50M; variation caused by the different average Mn oxidation state) decreases $E_{V_O^{\cdot\cdot}}$ by about 0.4 eV relative to bulk. The approach of $E_{V_O^{\cdot\cdot}}$ to the bulk value in deeper layers is depicted in Figure 1.

At 1000 K, the total difference of 1−1.2 eV in the surface $E_{V_O^{\cdot\cdot}}$ for the two terminations—for a given average Mn oxidation state—leads to a more than 5 orders of magnitude difference in the surface $V_O^{\bullet\bullet}$ concentrations (comparing surface-$E_{V_O^{\cdot\cdot}}$ for symmetrical LSM slabs without considering the different Mn oxidation states of *A*O and BO_2 terminations would strongly overestimate this ratio). The consequences for the ORR rate will be discussed below.

Bulk and surface $V_O^{\bullet\bullet}$ formation for LM has also been calculated in Ref. [26]. The use of U_{eff} = 4 eV leads to bulk $E_{V_O^{\cdot\cdot}}$ used in the present study, and being less positive by 1.2 eV than with U_{eff} = 0 eV (in line with the U_{eff} dependence reported in Ref. [25]). However, the energy differences between bulk and surface $V_O^{\bullet\bullet}$ are very similar to the behavior shown in Figure 1; correspondingly the relative difference of concentration between *A*O and BO_2 termination is comparable.

Also the adsorbed oxygen species are affected by Mn oxidation state and surface polarity [21]. This does not only refer to the adsorption sites (atop Mn for MnO_2; on "hollow" bridging positions above two (La,Sr) on (La,Sr)O) and energies, but even to the nature of the adsorbed species. This is indicated in Figure 2 [21]. Based on the charge and in particular the O−O bond length, the molecular adsorbed oxygen species on the LSM MnO_2 termination can be assigned to superoxide O_2^-. However, for the (La,Sr)O termination, significantly longer O−O bond lengths are found, which indicates a more negative charge (larger population of antibonding orbitals) up to peroxide O_2^{2-}. Atomic adsorbed O^- species on (La,Sr)O have a much more negative charge than on MnO_2 such that they can rather be assigned as O_{ad}^{2-}. In other words, the positive excess charge of the (La,Sr)O surface layer does not only disfavor formation of $V_O^{\bullet\bullet}$ but

Figure 1

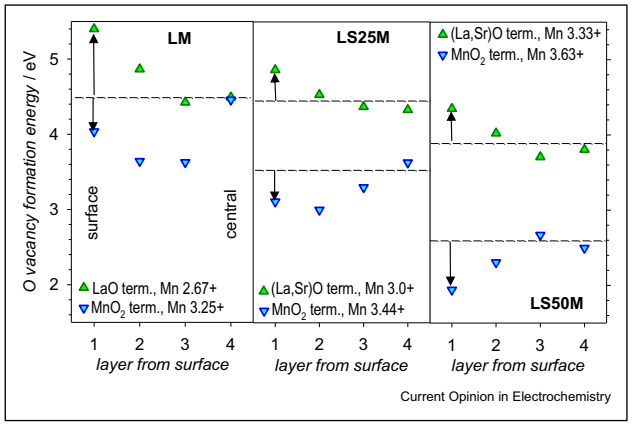

Vacancy formation energies in different layers of (001) terminated slabs of LM, LS25M, LS50M. The arrows indicate the energy difference relative to bulk with the same average Mn oxidation state (same for both terminations of LM, but different for the LS25M and LS50M terminations). Figure reproduced from Ref. [21].

Figure 2

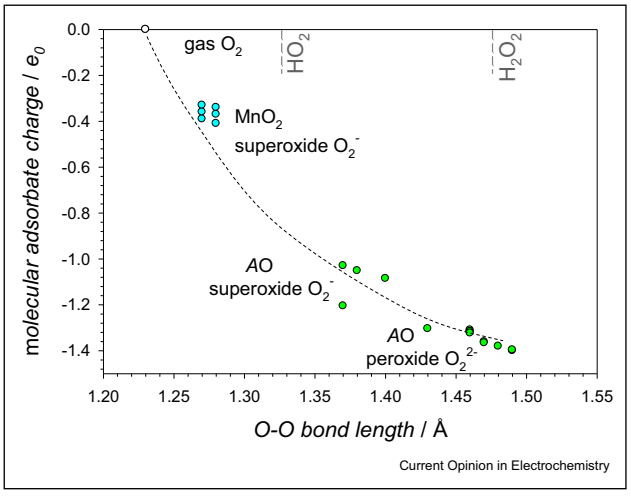

Charge of molecular oxygen adsorbates on (La,Sr)O termination and MnO_2 termination versus O−O bond length; for comparison also gaseous O_2, and experimental O−O bond lengths in HO_2, H_2O_2 are indicated [34]. Figure reproduced from Ref. [21].

in turn stabilizes stronger negatively charged adsorbed oxygen species.

The adsorption energies for molecular as well as atomic oxygen species ΔH_{ads} on LSM MnO_2 terminations are almost independent of the Mn oxidation state, being about −1 eV. This can be assigned to two trends, which apparently largely cancel each other: more favorable electron transfer to adsorbed O species, but also stronger electrostatic repulsion between negative adsorbates and negatively charged MnO_2 surface layer at less positive Mn oxidation state. From this ΔH_{ads} value, one can estimate an adsorbate coverage below approx. 1% for SOFC operation temperature of 1000 K (the comparably low coverages are caused by perceptible negative entropy of adsorption, estimated to −120 to −200 J/mol K [18] based on experimental data). On the (La,Sr)O termination, the adsorption energies are found to vary strongly with Mn oxidation state, from ≈ −4.5 eV (Mn 2.67+) to ≈ −2 eV (Mn 3.37+). Comparing the values at a fixed Mn + 3.25 oxidation state, ΔH_{ads} is about 1 eV more exothermic on (La,Sr)O. This should in principle increase the adsorbate coverages at 1000 K by several orders of magnitude. However, since the adsorbates are negatively charged, they experience increasing mutual electrostatic repulsion and the coverage is expected to level off at about 20% [18,21,30].

$(La,Sr)MnO_3$: energy profile and ORR kinetics

The energy profiles for the oxygen incorporation reaction on the AO termination based on the results from Refs. [18,21] are shown in Figure 3 (to have similar average Mn oxidation state, we compare LM MnO_2 ($Mn^{3.25+}$) and LS50M (La,Sr)O ($Mn^{3.33+}$) terminations). One has to keep in mind that the entropy change ≈ 2 eV at 1000 K due to loss of translational, rotational degrees of freedom of O_2) makes a significant contribution when going from the DFT energy calculated at zero Kelvin to Gibbs free energy for SOFC operation conditions.

The molecular oxygen adsorption forming O_2^-, O_2^{2-} is generally assumed to be a fast process on both terminations of redox-active perovskites as it requires only

Figure 3

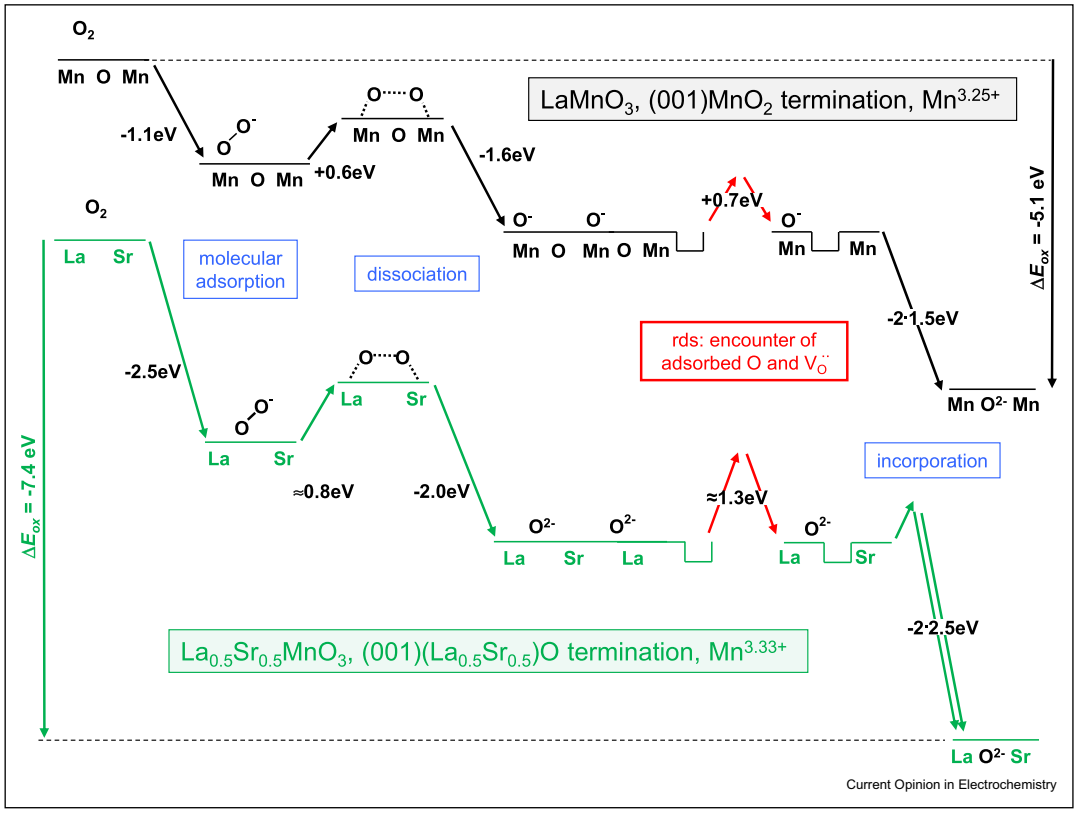

Calculated energy profiles for oxygen incorporation on the LM (001)MnO_2 (average Mn 3.25 + oxidation state) and LS50M (001) (La,Sr)O termination (Mn 3.33+); at zero K, no entropy effects included. The total reaction energy ΔE_{ox} for O incorporation into surface oxygen vacancies is less exothermic for LM MnO_2 because $V_O^{\bullet\bullet}$ are stabilized in the MnO_2 surface layer and destabilized at the (La,Sr)O surface. The encounter of MnO_2 and $O_{ad}^{-/2-}$ is the rate-determining step for both terminations. Reproduced from Refs. [4,21] with permissions from the PCCP Owner Societies.

electron transfer (also in other steps the respective electron transfers are expected to be fast). Owing to the low $V_O^{\bullet\bullet}$ concentrations even on the MnO_2 termination of LSM, molecular oxygen adsorption directly into a $V_O^{\bullet\bullet}$ can be neglected.

For LM MnO_2, the O—O dissociation barrier without $V_O^{\bullet\bullet}$ assistance was found to be 0.6 eV. At comparably low pO_2, the O—O dissociation was estimated to be rate determining, while for higher pO_2 the approach of a $V_O^{\bullet\bullet}$ to the formed O_{ad}^- was concluded to be the rds (the final incorporation of O_{ad}^- into a surface $V_O^{\bullet\bullet}$ occurs without barrier) [4,18].

For LS50M (La,Sr)O the atomic as well as molecular oxygen adsorption energies are quite negative (≈-2.4 eV for O_2^{2-}, 2·(-1.8 eV) for 2 O_{ad}^{2-}). Thus, the adsorbate coverages approach the plateau of approx. 20% mentioned before, with the O_{ad}^{2-} coverage exceeding that of O_2^{2-}. Similar to the MnO_2 surface, the incorporation of O_{ad}^{2-} into a neighboring $V_O^{\bullet\bullet}$ is considered not to have a large barrier, and thus to be fast. For LS50M (La,Sr)O the O_2 dissociation has a perceptible barrier of 0.8 eV. However, the encounter of the formed O_{ad}^{2-} species with a surface $V_O^{\bullet\bullet}$ is considered to be even slower, because the surface $V_O^{\bullet\bullet}$ concentration on this surface is extremely small. Diffusion of O_{ad}^{2-} along the surface has a high barrier of 1.3 eV, and also the approach of a $V_O^{\bullet\bullet}$ from bulk is comparably unfavorable (bulk $V_O^{\bullet\bullet}$ migration barrier 0.95 eV, and $V_O^{\bullet\bullet}$ less stable in surface layer by 0.4 eV than bulk (Figure 1)). Therefore, also for LS50M (La,Sr)O the encounter of the formed O_{ad}^{2-} species with a surface $V_O^{\bullet\bullet}$ is regarded as the rds [21].

So at comparably high pO_2 as relevant for an SOFC cathode material, for both LSM *A*O and MnO_2 termination the same reaction step determines the ORR rate. The ORR is expected to be much slower for the *A*O termination. On one hand, the more negative adsorption energies for atomic as well as molecular oxygen species on the *A*O termination can only partially be translated into higher $O_{2,ad}^{-/2-}$, $O_{ad}^{-/2-}$ concentrations because they run into the plateau value at about 20%. On the other hand, the surface $V_O^{\bullet\bullet}$ concentration is lower by more than 5 orders of magnitude on the *A*O termination. Combined with the higher effective migration barrier for O_{ad}^{2-}-$V_O^{\bullet\bullet}$ encounter, the ORR rate for the *A*O termination is estimated to be approx. 3 orders of magnitude lower than for MnO_2 at 1000 K [21]. This rough estimate indicates that even if most of a real SOFC cathode surface has a (La,Sr)O termination, even small patches of MnO_2 termination might still make a significant contribution to the overall ORR kinetics.

Finally we emphasize that the slow ORR rate of the (La,Sr)O surface is not due to difficulties of the electron transfer at this surface—as long as it is the *A*O termination of the perovskite structure, the hybridization of O and *B*-cation states still allows for easy electron transfer from the transition metal to adsorbed oxygen species. Only when multilayer separate $(La,Sr)O_x$ phases are formed, they will become electronically insulating.

(La,Sr)CoO_3: ORR mechanism and kinetics for *A*O and *B*O_2 termination

$La_{1-x}Sr_xCo_{1-y}Fe_yO_{3-\delta}$ perovskites have a bulk $V_O^{\bullet\bullet}$ concentration in the range of 0.01—0.1 under SOFC operation conditions [35]. This is one reason for their higher ORR rates compared to LSM (see e.g., [4,36]). A comparison of defects, adsorbates, and reaction barriers on the different surface termination has recently been made for $La_{0.5}Sr_{0.5}CoO_{3-\delta}$ (LS50C) using the GGA + U functional and an asymmetric 8-layer slab with one (001)SrO (mimicking Sr surface segregation) and one (001)CoO_2 surface. Finite temperature ORR rates for a large number of potential mechanisms have been determined from a microkinetic model [22].

Similar to the previously discussed results for LSM, the surface $V_O^{\bullet\bullet}$ concentration for LS50C is decreased on the SrO and increased on the CoO_2 termination. The increase of adsorbate concentrations on the LS50C SrO termination is less pronounced that on the LSM (La,Sr)O terminations, which might be related to the fact that the former carries no formal net positive charge. For the SrO surface, the rds was found to be the encounter of adsorbed atomic O species and surface $V_O^{\bullet\bullet}$ (similar to the LSM (La,Sr)O results), and correspondingly the ORR rate directly suffers from the decreased surface $V_O^{\bullet\bullet}$ concentration. For the CoO_2 surface, the $V_O^{\bullet\bullet}$-assisted dissociation of molecular adsorbed species was identified as the rds (the higher $V_O^{\bullet\bullet}$ concentration on LSC enables a vacancy-assisted dissociation, in contrast to LSM). Overall, at 650—800 °C and 20% O_2 the ORR rate on the LS50C CoO_2 surface is calculated to be about 2—3 orders of magnitude faster than on SrO. Again this suggests that small patches of *B*O_2 termination might significantly contribute to the overall ORR kinetics. Interestingly, for LS50C CoO_2 the absolute ORR rates are only about 1.5 orders of magnitude lower than the upper limit estimated from the gas-phase O_2 impact frequency. This emphasizes the potential of high ORR rates if a "clean" *B*O_2 termination could be stabilized [22].

ORR and OER kinetics of perovskites in aqueous environment

This article mainly focusses on the oxygen reduction reaction at the gas—solid interface. Here, we want to comment very briefly on the oxygen reduction or evolution from aqueous phase, which is important for water splitting/electrolysis and fuel cells operating at low temperatures. Ab initio modeling of the ORR and OER reaction in aqueous environment is challenging for

several reasons. While mixed conducting $ABO_{3-\delta}$ perovskites are attractive owing to lower materials cost than precious metals, they are usually not stable in acidic solutions. Even when exposed only to basic solution, severe cation leaching, surface reconstruction, or amorphization may occur (see e.g., Ref. [37]), making the real surface strongly differ from idealized configurations used in first principles calculations. In Ref. [38], the material's stability and activity were found to be closely related. Trends for the OER activity of binary oxides as well as perovskites have been calculated in Ref. [39]; however, based only on the energies of adsorbed intermediate species (not transition states). Reaction barriers and the sensitivity of the OER reaction to structural features such as the metal–metal distance have been considered more recently [40,41]. Owing to the reaction at the solid/water interface, solvation effects and protonation of intermediate species may become important, see for example, Refs. [42,43] Depending on the electronic structure of the perovskite (in particular the covalency of the transition metal–oxygen bond), the evolved oxygen is formed either only from adsorbed OH groups, or partly/completely from lattice oxygen (with the formed $V_O^{\bullet\bullet}$ filled from H_2O in a subsequent step) [44,45].

Conclusions

Recent *ab initio* calculations elucidated strong differences for the two possible polar (001) AO and BO_2 terminations of ABO_3 cathode perovskites. The surface oxygen vacancy concentration is drastically decreased on AO, while the concentrations of adsorbed atomic and molecular oxygen species are increased but reach a plateau value of $\approx 20\%$. For the AO terminations of $La_{1-x}Sr_xMnO_{3-\delta}$ and $La_{1-x}Sr_xCoO_{3-\delta}$, the encounter of surface $V_O^{\bullet\bullet}$ and adsorbed atomic O species is identified as the rate-determining step. Owing to the low-surface $V_O^{\bullet\bullet}$ concentration, the oxygen reduction rate is estimated orders of magnitude lower than for the respective BO_2 surface. Thus, even a small fraction of BO_2 may dominate the overall kinetics.

The comparison of results from different DFT studies shows that while absolute energies depend on the actual functional, the general trends (e.g., relative defect formation or adsorption energies) are rather comparable. While exactly modeling real oxide surfaces with high chemical and structural complexity (chemical inhomogeneity, higher-dimensional defects, etc.) is not possible, *ab initio* calculations still yield important mechanistic insight based on properly chosen model surfaces. In order to (at least approximately) describe the full complexity of real surfaces at SOFC operation conditions, a combination of zero temperature *ab initio* calculations with large scale finite temperature models such as Kinetic Monte Carlo approaches is required, as well as joint efforts with experimental studies.

Conflict of interest statement

Nothing declared.

Acknowledgments

This study was partly supported by M-ERA-NET project SunToChem (EK, YM). The computer resources were provided by Stuttgart Supercomputing Center (Project DEFTD 12939). Authors thank E. Heifets, M. M. Kuklja, M. Arrigoni, D. Morgan, R. Evarestov, and D. Gryaznov for fruitful discussions.

References

Papers of particular interest, published within the period of review, have been highlighted as:

* of special interest
** of outstanding interest

1. Wachsman E, Ishihara T, Kilner J: *MRS Bull* 2014, **39**:773.
2. Jacobson AJ: *Chem Mater* 2010, **22**:660.
3. Aguadero A, Fawcett L, Taub S, Woolley R, Wu KT, Xu N, Kilner JA, Skinner SJ: *J Mater Sci* 2012, **47**:3925.
4. Kuklja MM, Kotomin EA, Merkle R, Mastrikov YA, Maier J: *Phys Chem Chem Phys* 2013, **15**:5443.
5. * Kotomin EA, Merkle R, Mastrikov YA, Kuklja MM, Maier J. In *Chapter 6 in* computational Approaches to energy materials. Edited by Walsh A, Sokol AA, Catlow CRA, John Wiley & Sons; 2013.
Variety of computational methods for energy materials including SOFC is presented
6. Lee YL, Kleis J, Rossmeisl J, Shao-Horn Y, Morgan D: *Energy Environ Sci* 2011, **4**:3966.
7. Gao Z, Mogni LV, Miller EC, Railsback JG, Barnett SA: *Energy Environ Sci* 2016, **9**:1062.
8. * Adler SB, Chen XY, Wilson JR: *J Catal* 2007, **245**:91.
Good overview of discussion of reaction mechanisms based on experimental data
9. ** Piskunov S, Heifets E, Jacob T, Kotomin EA, Ellis DE, Spohr E: *Phys Rev B* 2008, **78**:121406.
Thermodynamic analysis of the relative stabilities of LSM surfaces
10. * Cai Z, Kubicek M, Fleig J, Yildiz B: *Chem Mater* 2012, **24**:1116.
Effects of phase separation and Sr segregation in $(La,Sr)CoO_3$ are studied
11. * Bucher E, Sitte W, Klauser F, Bertel E: *Solid State Ion* 2011, **191**:61.
Effects of Sr segregation are studied
12. Druce J, Tellez H, Burriel M, Sharp MD, Fawcett LJ, Cook SN, McPhail DS, Ishihara T, Brongersma HH, Kilner JA: *Energy Environ Sci* 2014, **7**:3593.
13. Jiang SP: *Int J Hydrogen Energy* 2019, **44**:7448.
14. Noguera C: *J Phys Condens Matter* 2000, **12**:R367.
15. ** Noguera C, Goniakowski J: *Chem Rev* 2013, **113**:4073.
Stability of polar surfaces in ionic solids is analyzed theoretically
16. * Setvin M, Reticcioli M, Poelzleiter F, Hulva J, Schmid M, Boatner LA, Franchini C, Diebold U: *Science* 2018, **359**:572.
Possible ways of perovskite polar surface reconstructions
17. Heifets E, Goddard III WA, Kotomin EA, Eglitis RI, Borstel G: *Phys Rev B* 2004, **69**. 035408.
18. * Mastrikov YA, Merkle R, Heifets E, Kotomin EA, Maier J: *J Phys Chem C* 2010, **114**:3017.
First principles modeling of ORR on LSM MnO_2 surfaces
19. Pilania G, Gao PX, Ramprasad R: *J Phys Chem C* 2012, **116**:26349.

20. Staykov A, Tellez H, Akbay T, Druce J, Ishihara T: *J Kilner Chem Mater* 2015, **27**:8273.

21. ** Mastrikov YA, Merkle R, Kotomin EA, Kulja MM, Maier J: *J Mater Chem A* 2018, **6**:11929.
ORR on two LSM terminations calculated and discussed

22. ** Cao Y, Gadre MJ, Ngo AT, Adler SB, Morgan D: *Nat Commun* 2019, **10**:1346.
Elementary reactions on (La,Sr)CoO_3 surfaces are calculated

23. Kohn W, Sham LJ: *Phys Rev* 1965, **140**:A1133.

24. Perdew JP, Burke K, Ernzerhof M: *Phys Rev Lett* 1996, **77**:3865.

25. Lee YL, Kleis J, Rossmeisl J, Morgan D: *Phys Rev B* 2009, **80**: 224101.

26. * Lee YL, Morgan D: *Phys Rev B* 2015, **91**:195430.
Detailed modeling of perovskite surfaces with defects

27. Pavone M, Munoz-Garcia AB, Ritzmann AM, Carter EA: *J Phys Chem C* 2014, **118**:13346.

28. Gryaznov D, Merkle R, Kotomin EA, Maier J: *J Mater Chem A* 2016, **4**:13093.

29. Kotomin EA, Mastrikov YA, Heifets E, Maier J: *Phys Chem Chem Phys* 2008, **10**:4644.

30. Fleig J, Merkle R, Maier J: *Phys Chem Chem Phys* 2007, **9**:2713.

31. Bjorheim TS, Arrigoni M, Saeed SW, Kotomin E, Maier J: *Chem Mater* 2016, **28**:1363.

32. Kuklja MM, Mastrikov YA, Jansang B, Kotomin EA: *J Phys Chem C* 2012, **116**:18605.

33. Mizusaki J, Mori N, Takai H, Yonemura Y, Minamiue H, Tagawa H, Dokiya M, Inaba H, Naraya K, Sasamoto T, Hashimoto T: *Solid State Ionics* 2000, **129**:163.

34. NIST: *computational chemistry comparison and benchmark database*. 14th ed. Washington DC: American Chemical Society; 2006.

35. Kawada T, Suzuki J, Sase M, Kaimai A, Nigara Y, Mizusaki J, Kawamura K, Yugami H: *J Electrochem Soc* 2002, **149**:E252.

36. Baumann FS, Fleig J, Cristiani G, Stuhlhofer B, Habermeier HU, Maier J: *J Electrochem Soc* 2007, **154**:B931.

37. May KJ, Carlton CE, Stoerzinger KA, Risch M, Suntivich J, Lee Y-L, Grimaud A, Shao-Horn Y: *J Phys Chem Lett* 2012, **3**:3264.

38. Rong X, Parolin J, Kolpak AM: *ACS Catal* 2016, **6**:1153.

39. Man IC, Su HY, Calle-Vallejo F, Hansen HA, Martinez JI, Inoglu NG, Kitchin J, Jaramillo TF, Norskov JK, Rossmeisl J: *ChemCatChem* 2011, **3**:1159.

40. Dickens CF, Kirk C, Norskov JK: *J Chem Phys C* 2019, **123**: 18960.

41. Pittkowski R, Krtil P, Rossmeisl J: *Curr Op Electrochem* 2018, **12**: 218.

42. Gauthier J, Dickens CF, Chen LD, Doyle AD, Norskov JK: *J Phys Chem C* 2017, **121**:11455.

43. Yoo JS, Liu Y, Rong X, Kolpak AM: *J Phys Chem Lett* 2018, **9**: 1473.

44. Mefford JT, Rong X, Abakumov AM, Hardin WG, Dai S, Kolpak AM, Johnston KP, Stevenson KJ: *Nat Commun* 2016, **7**: 11053.

45. Grimaud A, Diaz-Mprales O, Han B, Hong WT, Lee YL, Giordano L, Stoerzinger KA, Koper MTM, Horn Y Shao: *Nat Chem* 2017, **9**:457.

Institute of Solid State Physics, University of Latvia as the Center of Excellence has received funding from the European Union's Horizon 2020 Framework Programme H2020-WIDESPREAD-01-2016-2017-TeamingPhase2 under grant agreement No. 739508, project CAMART²